High-resolution study of 0^+ and 2^+ excitations in ^{168}Er with the (p, t) reaction

D. Bucurescu,[1,*] G. Graw,[2] R. Hertenberger,[2] H.-F. Wirth,[3] N. Lo Iudice,[4] A. V. Sushkov,[5] N. Yu. Shirikova,[5] Y. Sun,[6,7,8] T. Faestermann,[3] R. Krücken,[3] M. Mahgoub,[3] J. Jolie,[9] P. von Brentano,[9] N. Braun,[9] S. Heinze,[9] O. Möller,[9] D. Mücher,[9] C. Scholl,[9] R. F. Casten,[10] and D. A. Meyer[10]

[1]*Horia Hulubei National Institute of Physics and Nuclear Engineering, P.O. Box MG-6, R-76900 Bucharest, Romania*
[2]*Sektion Physik, Ludwig Maximilians Universität München, Am Coulombwall 1, D-85748 Garching, Germany*
[3]*Physik Department, Technische Universität München, D-85748 Garching, Germany*
[4]*Dipartimento di Scienze Fisiche, Università di Napoli "Federico II" and Istituto Nazionale di Fisica Nucleare, Monte S Angelo, Via Cintia I-80126 Napoli, Italy*
[5]*Bogoliubov Laboratory of Theoretical Physics, Joint Institute for Nuclear Research, RU-141980 Dubna, Russia*
[6]*Department of Physics and Joint Institute for Nuclear Astrophysics, University of Notre Dame, Notre Dame, Indiana 46556, USA*
[7]*Department of Physics, Tsinghua University, Beijing 100084, China*
[8]*Department of Physics, Xuzhou Normal University, Xuzhou, Jiangsu 221009, China*
[9]*Institut für Kernphysik, Universität zu Köln, D-50937 Köln, Germany*
[10]*Wright Nuclear Structure Laboratory, Yale University, New Haven, Connecticut 06520-8124, USA*

(Received 9 March 2006; published 29 June 2006)

Excited states in the deformed nucleus ^{168}Er have been studied with high-energy resolution, in the (p, t) reaction, with the Munich Q3D spectrograph. A number of 25 excited 0^+ states (four tentative) and 63 2^+ states have been assigned up to 4.0 MeV excitation energy. This unusually rich characterization of the 0^+ and 2^+ states in a deformed nucleus, close to a complete level scheme, offers a unique opportunity to check, in detail, models of nuclear structure that incorporate many excitation modes. A comparison of the experimental data is made with two such models: the quasiparticle-phonon model (QPM), and the projected shell model (PSM). The PSM wave functions appear to contain fewer correlations than those of the QPM and than required by the data.

DOI: 10.1103/PhysRevC.73.064309 PACS number(s): 21.10.−k, 25.40.Hs, 27.70.+q, 21.60.−n

I. INTRODUCTION

The full microscopic description of low-lying excitations of well-deformed nuclei, such as in the rare earths, is still not achieved, since they may arise from complicated manifestations of different collective and single-particle degrees of freedom. For example, even the nature of the lowest excited 0^+ states in such nuclei has been discussed as a rather controversial subject (see Ref. [1] and references therein). The lowest collective 0^+ and 2^+ modes expected in a simple-minded picture in a deformed nucleus are those due to the two types of quadrupole vibration about the equillibrium shape, the so-called β and γ vibrations, which lead to the well-known $K^\pi = 0^+$ and $K^\pi = 2^+$ bands. At higher excitation, one expects multiphonon states built on these β and γ phonons. Above the pairing gap there will be many states composed of quasiparticle excitations. The real situation may be rather more complicated, since the nuclear residual interactions will mix these excitations. Detailed experimental data on the properties of many excited states in deformed nuclei require, for their understanding, the use of microscopic models that can handle in a realistic manner such a complicated many-body problem. A full quantum-mechanical treatment of a many-body system is difficult because of the large number of degrees of freedom. In the terminology of the shell model, the configuration space in which the Hamiltonian is to be diagonalized is extremely large in heavy nuclei. A more limited realistic goal is to identify the main components of the low-lying, low-spin states and understand their mixing. Thus, if we limit our interest to a certain class of states (e.g., moderate excitation energies and low spins, as discussed in this paper), a shell-model-type calculation may be carried out by using a set of a few well-selected configurations. This is the basic idea behind the methods we apply in this study. The two models used in this paper represent two different shell model truncation schemes.

This situation was rather dramatically emphasized by the improvement of experimental techniques. For example, sensitive γ-ray measurements have allowed identification of the long-sought multiphonon states, and their measured properties have been important for the improvement of the nuclear models. Another example is the use of high-precision transfer reaction experiments, which can identify a large number of states. Such an experiment, using the (p, t) reaction, disclosed 13 excited 0^+ states in the deformed nucleus ^{158}Gd [2], up to 3.1 MeV excitation, a number that exceeded the expectations of most current theoretical estimations. This stirred considerable interest and several theoretical approaches attempted to explain these findings: the *spdf* interacting boson model (IBM) [3], the projected shell model (PSM) [4], the quasiparticle-phonon model (QPM) [5], and a model including monopole pairing, quadrupole-quadrupole, and spin-quadrupole forces in the framework of the random phase approximation (RPA) [6]. A similar study in the actinide nuclei also revealed large numbers of excited states [7]. Recent experiments of the same type were systematically made on many nuclei between ^{152}Gd and ^{192}Hg and revealed a large number of excited 0^+ states, whose systematics is not yet understood in detail [8].

*Electronic address: bucurescu@tandem.nipne.ro

New theoretical investigations of some of these data, based on the QPM, followed soon [9].

The experimental data reported here for the nucleus ^{168}Er are part of the above mentioned extended (p, t) reaction study campaign [8] but are the best studied case. The experiments on ^{168}Er differed from those on the other nuclei in that detailed angular distributions were measured at seven angles and up to an excitation energy of about 4.1 MeV. The richness of the data obtained from these measurements, which provides an impressive number of 0^+ and 2^+ states, means that this nucleus remains one of the best known deformed nuclei.

The nucleus ^{168}Er has been considered one of the best experimentally studied deformed nuclei and therefore a prefered ground for testing nuclear models. The ENSDF (Evaluated Nuclear Structure Data File, maintained by the National Nuclear Data Center, Brookhaven National Laboratory) database lists indeed an impressive number of well-characterized levels and an equally impressive number of rotational bands deduced from the data [10]. We shall quote only a few of the experimental papers (with relevance to the present work) that contributed to this knowledge. In an early study with the (p, t) and (t, p) reactions [11] three excited 0^+ states were identified up to 1.833 keV excitation energy; our present study confirms both the energy and the excitation strengths of these states. Very important for a complete determination of the level scheme at low spins and up to low-to-moderate level density, corresponding to about 2 MeV excitation, was the series of three (n, γ) studies [12–14]. These studies, however, have many difficulties above $\sim$2 MeV of excitation energy, and completeness is rapidly lost (see the comparison in refs. [12–14] relative to Ref. [15]). These works emphasized the usefulness of such detailed knowledge of the level schemes in several directions that are of current interest, such as the study of multiphonon states, the onset of chaos at energies above the pairing gap and the extension of nuclear structure model interpretations into the region above the pairing gap. The question of the onset of chaos in this nucleus has generated much debate, revealing the importance of having a reliable ensemble of levels [16,17]. ^{168}Er is also the first nucleus in which definite evidence for the existence of a two-phonon collective state was found (the 4^+ $\gamma\gamma$ vibration state) [18], based on lifetime measurements with the GRID technique in the (n, γ) reaction. The positive anharmonicity of this 2γ mode $[E(4^+_{2\gamma})/E(2^+_\gamma) = 2.52]$ is one of the largest known in the rare-earth region [19]. Other subsequent GRID lifetime measurements with the (n, γ) reaction precisely characterized the $K^\pi = 0^+$ band based on the 0^+_1 state at 1217 keV and ruled out a pure β-vibrational mode [20]. Finally, the (γ, γ') photon scattering work [21] established the low-lying dipole excitations (1^+ and 1^- states) in this nucleus. It is worth mentioning that detailed experimental studies are also very important to identify and exploit different paradigms of nuclear structure, such as dynamical symmetries or critical point symmetries. In this respect, ^{168}Er has been discussed as a possible good candidate for the Y(5) symmetry, which represents the critical point of a shape transition in the γ degree of freedom (axially to triaxially deformed shape transition) [22].

The present work reports the results of a high-precision, high-resolution (p, t) reaction study of ^{168}Er. Only the results concerning 0^+ and 2^+ states up to 4.1 MeV excitation will be discussed (close to 100 excited states). It would be impossible to present exhaustively both the experimental knowledge and the theoretical understanding of this rather well studied nucleus. The more restricted purpose of this paper is twofold. First, the experimental results of the two-neutron transfer reaction study will be presented, and the outstanding potential of such an approach for a quasi-complete determination of low-spin levels (0^+ and 2^+) is emphasized. We stress that a key element in achieving the experimental goals of this study is the high-energy resolution and precision of the spectrometer used to detect the outgoing tritons. Second, a comparison of these detailed data is presented with two state-of-the-art theoretical approaches: the quasiparticle-phonon model (QPM) [23], and the projected shell model (PSM) [24].

II. EXPERIMENTAL DETAILS

A. Measurements

The experiment was performed with an unpolarized proton beam of 25.0 MeV delivered by the Tandem accelerator of the Meier Leibnitz Laboratory of the University and Technical University in Munich. The Er_2O_3 target was 98% enriched in ^{170}Er, with a thickness of 120 μg/cm^2, deposited on a 13 μg/cm^2 carbon backing. The most important impurity of the target was ^{168}Er (1.1%), from which only the peaks corresponding to the ground and 2^+_1 states of ^{166}Er were clearly identified.

The reaction products were analyzed with the Munich Q3D spectrograph [25] and then detected in a 1 m long cathode strip focal plane detector [26,27], which made ΔE-$E_{\rm rest}$ particle identification and position determination. The acceptance of the spectrograph was 11.1 msr (horizontal$\times$vertical of $\pm$20 mm $\times$ $\pm$20 mm), except for the most forward angle (5°), where it was 6.1 msr ($\pm$10 mm $\times$ $\pm$20 mm). Typical beam currents were from 0.5 to 1.3 μA.

Spectra were measured at 7 angles: 5°, 10°, 14°, 17.5°, 23°, 30°, and 37.5°. For each angle, three spectra were collected, with three different magnetic settings of the spectrograph, such as to cover the excitation energy range from 0 to $\sim$4.1 MeV, the magnetic field values being chosen in such a way that these runs had overlaps in energy. The energy calibration was performed by using well-known peaks from ^{168}Er [10] and by measuring the reactions ^{172}Yb(p, t) [28] and ^{208}Pb(p, t) [29] under the same magnetic settings. The different runs were normalized to the beam current integrated into a Faraday cup placed behind the target.

Figure 1 shows, as an example, the three spectra measured at the laboratory angle of 10°. A FWHM energy resolution of 4–6 keV, depending somewhat on the position in the focal plane, was obtained for the whole measured energy range. The spectra were virtually background free. Under these conditions, more than 200 excited states were observed up to 4.07 MeV excitation, and angular distributions were determined for most of them.

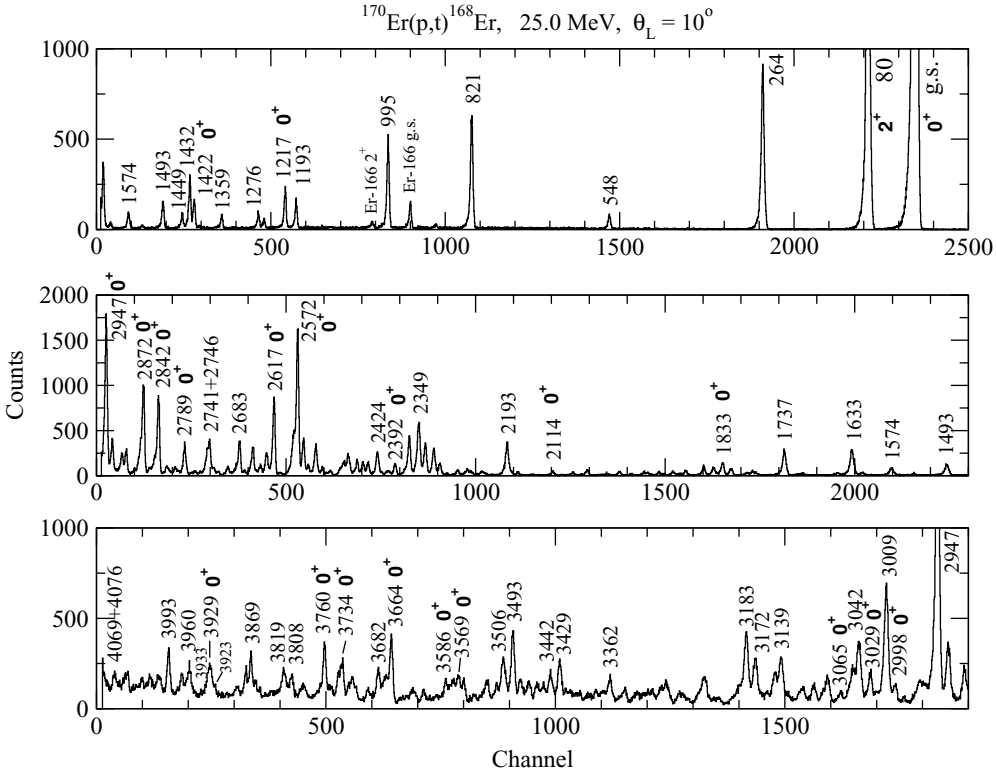

FIG. 1. Spectra measured at an angle $\theta_L = 10^\circ$ for the $^{170}\mathrm{Er}(p,t)^{168}\mathrm{Er}$ reaction at 25.0 MeV. The spectra have been measured for three different magnetic field settings of the Q3D spectrograph, for integrated charges of 7.8 mC (above), 10.8 mC (middle), and 13.6 mC (bottom), for a ± 20 mm $\times \pm 20$ mm opening (solid angle 11.1 msr). Peak labels represent excitation energies in keV. The states assigned as 0^+ are marked.

B. DWBA analysis and experimental results

The determination of the value of the transferred angular momentum (L) and spin ($J = L$) for each level in the final nucleus ^{168}Er relies on a comparison of the experimental angular distributions with predictions of DWBA calculations. The assignment of the $L = 0$ transfer (0^+ states) is particularly straightforward, since in the (p,t) reaction at our incident energy, for a direct, one-step process, the angular distribution is strongly forward peaking and has a sharp minimum around 17°, rather different from that of $L \neq 0$ transitions whose first maximum shifts systematically toward higher angles with increasing L. Rather unambiguous assignments could be made for 0^+ and 2^+ states, and these will be discussed below.

The DWBA calculations were performed with the code CHUCK3 [30]. The optical model parameters for these DWBA calculations were taken from Ref. [31]. In principle, the transfer of the two neutrons coupled to spin 0 should contain the contribution of different j values of the two particles. However, we do not know the relative contributions of different j^2 neutron pair transfers to the final state of interest. Therefore our approach is more limited: we performed calculations with the simplest form factor, which assumes just one j^2 configuration. This will limit the information that we can get about the structure of the excited states, which is contained in the intensity with which each state is populated in our reaction.

Typical angular distributions calculated in this way for the different neutron orbitals expected to contribute in our case ($1h_{9/2}$, $1i_{13/2}$, $2f_{7/2}$, $2f_{5/2}$, $3p_{3/2}$) are shown in Fig. 2. There are two effects to be considered in the discussion of the results of such an analysis. First, as shown in Fig. 2, the shape of the $L = 0$ and $L = 2$ angular distributions does not practically depend on the chosen form factor, whereas the absolute value of the calculated cross sections does. Second, the excitation energy of each state was explicitly taken into account, such that the binding energies of the two neutrons matched the energy of the outgoing triton, thus obtaining a kinematic correction of the cross section. This kinematic correction, shown in Fig. 2, depends on the form factor, too.

By normalizing the calculated cross sections to the experimental data, we obtain, in principle, a kind of "spectroscopic factor"; however, since we do not know the dominant transfer for each state, for any chosen form factor the corresponding spectroscopic factor obtained may differ strongly from the actual one. To minimize the errors we make in this way, we have used for all states an $f_{7/2}^2$ form factor that provides an average behavior (see Fig. 2). Since, undoubtedly, different excited states have quite different structures, the strengths obtained in this way can only qualitatively remove the kinematics effects of the reaction and give only a crude guide to transition matrix elements. One should keep these limitations in mind when comparing model predictions: the quantities that we extract from our data in this way are in fact Q-independent cross sections—that is, we roughly compare the cross sections at a constant Q value, but they can give only a rough indication of the spectroscopic factors.

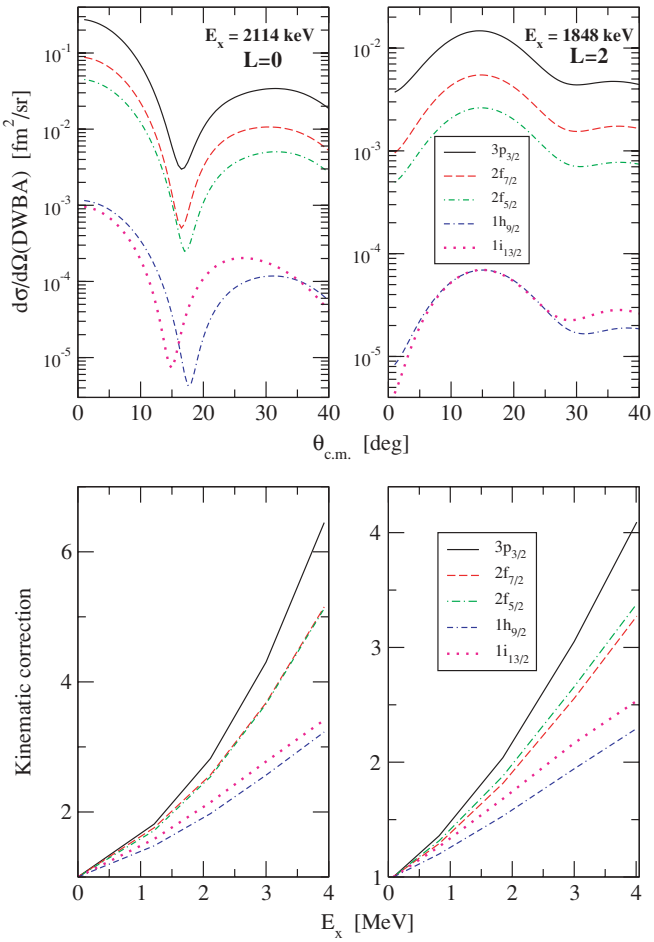

FIG. 2. (Color online) Upper part, $L = 0$ and $L = 2$ angular distributions predicted by DWBA calculations with a form factor that assumes the two neutrons coming from only one orbital, as specified. Lower part, kinematic correction for the same DWBA calculations. This is defined as the relative cross section values at the same angle (5° for $L = 0$ and 15° for $L = 2$, respectively), as a function of the excitation energy of the final state.

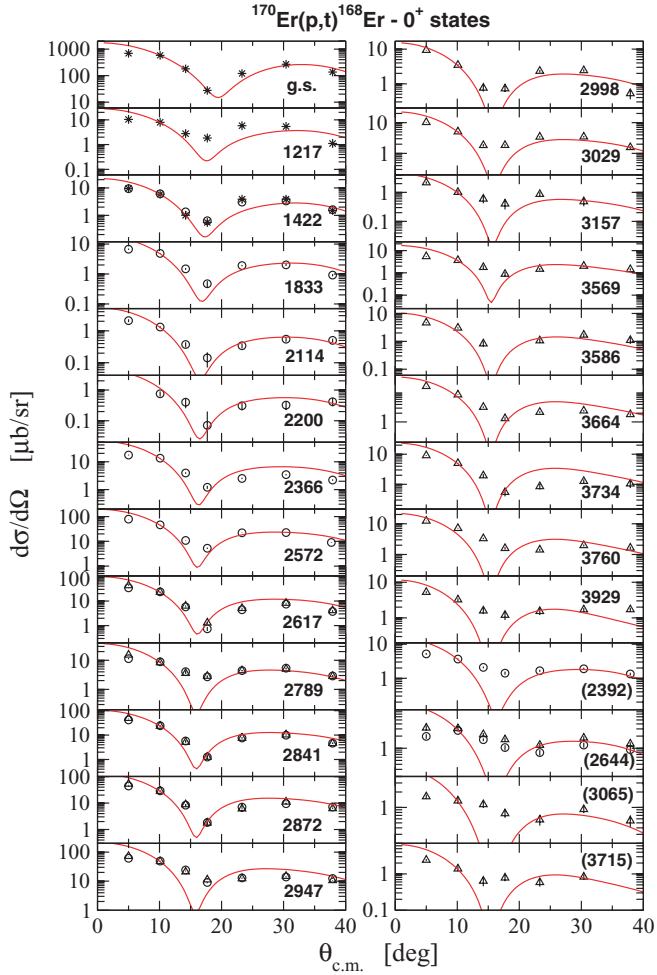

FIG. 3. (Color online) Angular distributions for ^{168}Er states assigned as 0^+. The states are labeled with their energy in keV (see also Table I). Parentheses indicate tentative assignment. Two different symbols occuring for some states indicate different runs (measurements with different magnetic settings). The continuous curves represent DWBA calculations with a $f^2_{7/2}$ form factor, normalized to the data.

Figure 3 shows the states for which a 0^+ assignment was established. The assignment of all these states is rather direct, even without DWBA curves, by comparison with the angular distributions of the ground state (g.s.) and a few other known 0^+ states, at 1217, 1422, and 1833 keV. Above 1833 keV there was no other known 0^+ state [10], therefore all assignments above 2 MeV excitation energy made in the present work are new. The four graphs in the bottom of Fig. 2 present tentative 0^+ assignments: the angular distributions have forward peaking, but in general are more flat than the rest in the figure, which may indicate contribution from two-step processes (which do not peak forward). These states have rather low cross sections, below 5 μb/sr at 5°. In the case of the 2392.1 keV state, the angular distribution may be more flat due to the contribution of the known 2^+ state at 2393.6 keV [10] which could not be separated. Table I gives a detailed account of all the assigned 0^+ states, including the relative spectroscopic strengths.

Figure 4 shows, in addition, another 7 excited states, at 3116.8, 3147.2, 3312.8, 3529.0, 3581.1, 3682.5, and 3696.7 keV, which are also forward peaking. Since for both one- and two-step $L > 0$ transfers there is no increase at forward angles, these might represent also 0^+ states. These states also have rather small cross sections, around 2–3 μb/sr at 5°; therefore their spectroscopic strengths would be at most of the order of ∼0.2%–0.3% (with the g.s. transition normalized to 100%).

As a paranthesis, we add a comment related to the 1^+ states. Such states cannot be populated in a $L = 0$ one-step process, since the two transferred neutrons are in a spin 0 state (s state), and for a two-step process we do not expect forward peaking. Nevertheless, since there are many 1^+ states known in ^{168}Er [21], we checked whether any of the 0^+ states assigned by us coincides with a known 1^+ state. A few of our states have energies that are not far from the values (with unknown error) given in Ref. [21]: thus, the tentative 2643.2 keV state

TABLE I. 0^+ states of ^{168}Er observed in the present experiment (see also Fig. 3). Tentative 0^+ assignments are indicated by parentheses. Other possible 0^+ states, with forward peaking but not typical angular distributions are shown in Fig. 4. The last column gives values of relative reaction strength ("spectroscopic factors") as extracted from the data by normalizing the DWBA calculations performed with a simple $f^2_{7/2}$ form factor (see the discussion in Secs. II B and II C).

E_x (keV) NNDC [10]	E_x (keV)	$\frac{d\sigma}{d\Omega}(5^\circ)$ ($\frac{\mu b}{sr}$) present data	Relative strength
0	0	693(10)	100
1217.160(14)	1217.1(1)	10.4(5)	0.91
1422.10(3)	1421.9(2)	9.5(5)	0.65
1833.54(11)	1833.7(2)	6.7(4)	0.46
	2114.1(4)	2.1(2)	0.11
	2200.6(4)	0.75(14)	0.10
	2366.2(2)	17.4(6)	1.06
	2392.1(2)[a]	5.2(3)	0.30
	2572.5(2)	78.6(12)	3.39
	2617.4(2)	43.0(17)	1.71
	2644.1(6)	3.2(4)	0.22
	2789.2(4)	15.4(4)	0.59
	2842.1(3)	49.1(11)	1.62
	2872.2(3)	53.0(9)	1.95
	2947.4(4)	72.3(11)	3.15
	2998.3(6)	9.3(3)	0.23
	3028.6(6)	10.2(3)	0.33
	3065.0(7)	1.6(2)	0.09
	3157.5(7)	2.2(2)	0.06
	3569.4(10)	5.5(3)	0.20
	3586.3(10)	4.7(2)	0.12
	3663.9(10)	16.9(3)	0.40
	3714.9(10)	2.4(2)	0.08
	3734.4(10)	9.1(3)	0.27
	3760.1(10)	12.3(3)	0.24
	3928.9(10)	5.2(4)	0.12

[a]The angular distribution could be affected by the known 2^+ state at 2393.6 keV [10].

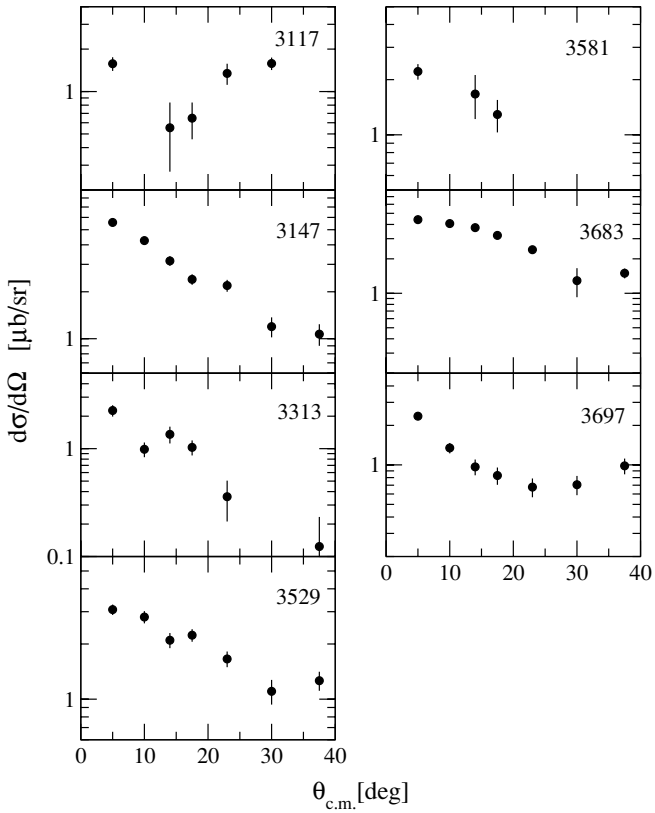

FIG. 4. Angular distributions of states in ^{168}Er that have not been assigned, but, because of the forward peaking, may be 0^+ states.

(Table I) coincides in energy with the 1^+ state at 2643 keV [21]; 2789.2 keV is close to 2792 keV; 3586.3 keV to 3591 keV; and 3663.9 keV to 3657 keV. Assuming errors of 1–2 keV for the energies of Ref. [21], and also considering the angular distribution shape and the relatively large cross sections of our states, it is very unlikely that any of these assigned 0^+ states is one of the known 1^+ states.

Figure 5 displays the angular distributions of the states that have been assigned as 2^+. The $L = 2$ DWBA calculated curves compare quite well with the measured shapes. Comparison with both calculated and empirical (for well-known 2^+ states) angular distributions have been used to make new $L = 2$ assignments. The possibility of incorrectly assigning $L = 2$ to a state with $L \neq 2$ must also be considered. While the $L = 2$ transitions are rather different from those with $L = 0$ and $L = 4$, they are closer in shape to the $L = 3$ ones. However, the $L = 3$ angular distributions peak at a larger angle (about 18°, compared to approximately 15° for $L = 2$) and their maximum is broader. We have carefully compared the shapes of our $L = 2$ assigned angular distributions with those of well-known 3^- states (clean angular distributions were observed for the states at 1431, 1633, 1914, 2022, and 2263 keV [10]) and with the calculated ones (Fig. 5), and the 2^+ assignments listed in Table II look reasonably safe. Mixing of configurations and coupled channels effects may lead to more complicated angular distributions, which make L assignments for states with flatter angular distributions more difficult. Therefore the cases without a clear diffraction like pattern were left out. The observation made above with the 1^+ states applies also to the $L = 2$ states. There are a few states assigned as 1^+ [21] (energies 2827, 3048, 3341, 3357, 3457, and 3806 keV [10]), that are close to states that we assigned as 2^+ (see, for comparison, Table II), but, since our states have relatively large cross-sections and rather clean $L = 2$ type angular distribution, it is unlikely that the 2^+ assignment is wrong.

There are 66 states assigned as 2^+ up to 4.075 MeV excitation (including the state at 2450.5 keV with tentative assignment). As mentioned above, the known 2^+ state at 2393.6 keV [10] could not be resolved from a 0^+ state with about the same energy. There is an excited state at 2174.0 keV that could correspond to the 2177.8 (2^+) state [10]; however, its angular distribution is rather structureless and we could not confirm a 2^+ assignment. Out of the 2^+ states known up to 2.4 MeV, only the state at 2137.1 keV [10] was not observed. The level observed at 2424.1 keV has been considered the same

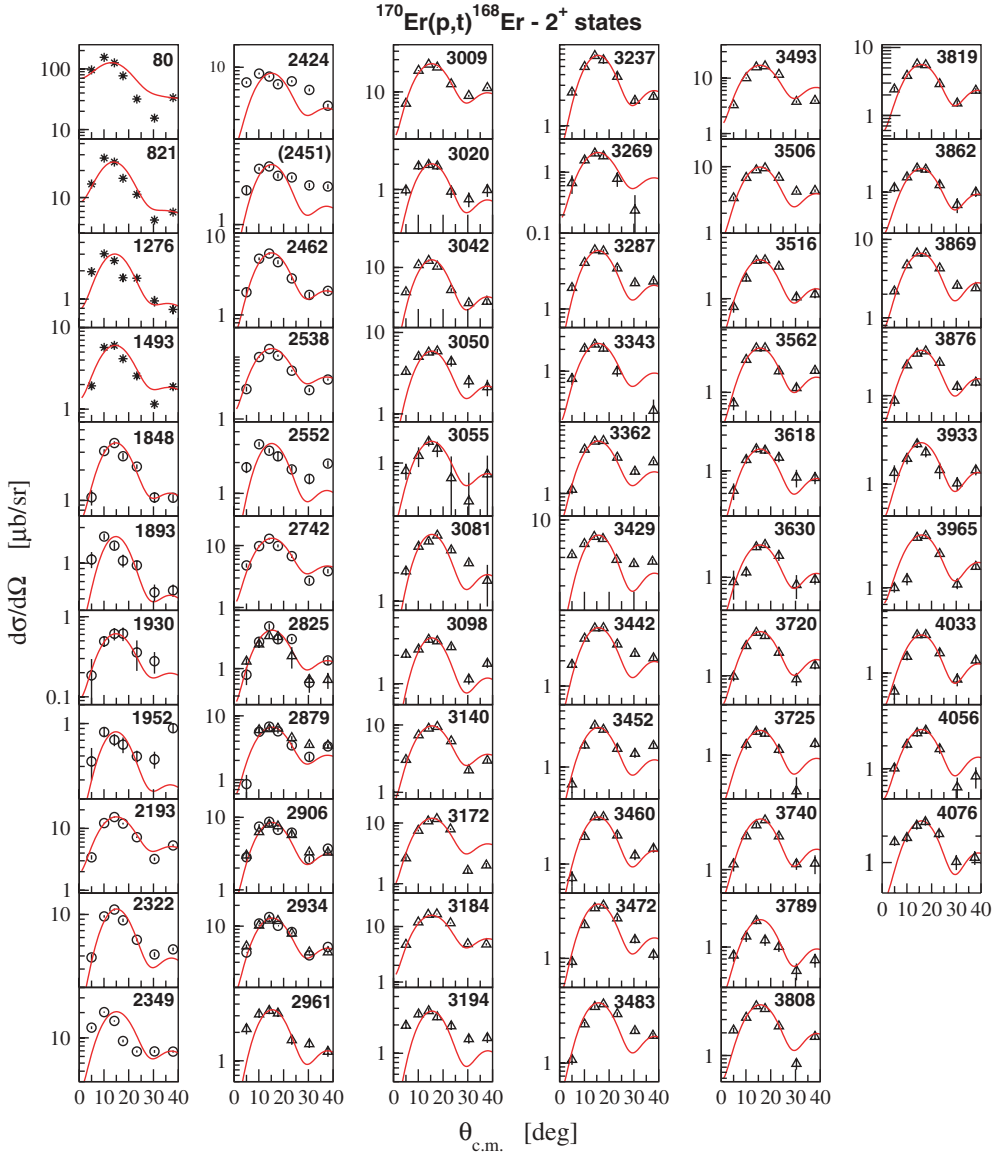

FIG. 5. (Color online) Same as Fig. 3, for states assigned as 2^+.

with the known 2^+ state at 2425.4 keV [10], but, since the shape of its angular distribution appears to contain some unknown contribution, the spectroscopic strength given for this state in Table II is only an upper limit. A last comment concerns a state observed by us at 2322.2 keV, which has a rather clean $L = 2$ pattern (Fig. 5), so that it appears to have very little influence from the known 3^- level at 2323.2 keV [10]. Table II gives details concerning the 2^+ states.

In summary, up to 4 MeV excitation, 26 states have been assigned as 0^+ (4 only tentatively) and 63 states have been assigned as 2^+ (one not observed due to superposition with a 0^+ state). Several other states between 3.1 and 3.7 MeV might be also 0^+ states. Altogether, from more than 200 states identified in this work up to 4.07 MeV, about 100 are 0^+ and 2^+. Most of the 0^+ states are newly observed, while from the known 2^+ states up to about 2.4 MeV only one was not observed.

Since such a large number of states has been observed, a legitimate question is, how close are we to a "complete" determination of the 0^+ and 2^+ states up to the investigated excitation energy of 4.1 MeV. The (p, t) reaction has features that dictate characteristic selection rules for the observed transfers: states that do not contain pairing correlations as in the ground state of the target should, in principle, not be excited. However, owing to mixing effects that are always present, we do not expect that such selection rules are strictly obeyed, except in very special cases. Since we were able to measure rather weakly populated states, with cross sections as low as $\sim 1\,\mu$b/sr (around 0.1% of the ground state), in spectra practically without background, and with a very good energy resolution, close to that of γ-ray spectroscopy with Germanium detectors, it is very likely that we have observed most of the 0^+ and 2^+ states in the energy region from 0–4 MeV. This is partly confirmed by a comparison with the

TABLE II. 2^+ states of ^{168}Er observed in the present study (see also Fig. 5). Tentative assignments are indicated by parentheses. The last column gives values of relative reaction strength ("spectroscopic factors") as extracted from the data by normalizing the DWBA calculations performed with a simple $f_{7/2}^2$ form factor (see the discussion in Secs. II B and II C).

E_x (keV) NNDC [10]	E_x (keV)	$\frac{d\sigma}{d\Omega}(14^\circ)$ ($\frac{\mu b}{sr}$) present data	Relative strength
79.804(1)	79.8(1)	126(2)	100
821.169(2)	821.2(1)	24.9(4)	15.1
1276.274(2)	1276.3(1)	2.6(2)	1.55
1493.135(4)	1493.2(1)	6.0(5)	2.88
1848.351(5)	1848.2(2)	3.7(2)	1.56
1893.102(5)	1893.0(2)	1.4(1)	0.70
1930.392(4)	1930.1(3)	0.6(1)	0.25
	1952.2(7)	0.7(1)	0.34
2137.08(9)	—	not obs.	—
(2177.790(15))	—		
2193.20(4)	2193.0(1)	15.3(4)	5.77
	2322.2(2)	11.14(26)	4.03
	2349.3(3)	15.9(3)	7.33
2393.60(9)	—[a]	—	—
2425.42(6)	2424.1(2)	7.5(2)	2.90
	(2450.5(3)	4.4(2)	1.61)
	2461.8(2)	5.6(2)	1.98
	2538.2(3)	1.3(3)	4.59
	2552.2(3)	2.6(2)	1.03
	2741.9(4)	12.9(5)	4.15
	2825.0(4)	4.1(4)	1.11
	2878.9(4)	6.8(7)	2.01
	2906.0(4)	8.7(6)	2.54
	2934.1(5)	13.5(7)	3.90
	2961.2(6)	3.4(3)	1.04
	3009.0(3)	525.5(5)	7.60
	3020.0(5)	2.0(2)	0.59
	3042.4(5)	12.0(3)	3.57
	3049.9(5)	5.7(3)	1.72
	3055.1(5)	1.9(3)	0.55
	3081.3(6)	4.3(3)	1.46
	3098.4(6)	2.9(2)	0.88
	3139.6(6)	8.8(3)	2.70
	3172.5(7)	10.7(3)	3.35
	3183.7(8)	16.4(4)	4.45
	3194.4(8)	2.8(2)	0.78
	3237.2(8)	6.7(3)	1.83
	3269.4(8)	2.0(2)	0.57
	3286.8(8)	5.0(2)	1.35
	3342.9(10)	2.3(2)	0.64
	3361.9(10)	4.9(2)	1.32
	3429.2(10)	6.6(3)	1.79
	3441.7(10)	4.9(2)	1.29
	3451.6(10)	3.3(2)	0.81
	3459.9(10)	3.6(2)	0.95
	3471.6(10)	4.0(2)	1.15
	3482.6(10)	4.7(2)	1.34
	3493.3(10)	15.8(3)	4.35
	3506.3(10)	8.9(3)	2.52
	3515.7(12)	3.3(2)	0.88
	3561.9(12)	3.9(2)	1.00
	3617.6(12)	1.9(2)	0.49
	3629.9(12)	2.6(3)	0.69
	3720.0(15)	3.9(3)	0.99
	3725.2(15)	2.1(2)	0.53
	3740.4(15)	3.7(3)	1.07
	3789.5(15)	2.2(2)	0.54
	3808.5(15)	4.5(2)	1.11
	3819.4(15)	5.7(2)	1.33
	3861.9(15)	2.2(2)	0.52
	3868.7(15)	6.7(3)	1.56
	3876.3(15)	3.6(2)	0.93
	3933.0(15)	3.2(3)	0.76
	3964.9(15)	4.6(3)	1.13
	4033.5(15)	3.0(2)	0.68
	4055.9(15)	2.9(3)	0.74
	4075.6(15)	2.6(3)	0.67

[a]The known 2393.6 keV level [10] could not be resolved from the 0^+ state at 2392.1 keV (see Table I and Fig. 2).

states known before from different studies [10], and especially those determined with the nonselective reaction (n,γ) [12–14]. Only three 0^+ excited states were known up to 1833 MeV, so all the states above this energy are newly observed. The observation of very weakly excited 0^+ states at higher energies presents a rather delicate problem, as shown by the seven states between 3.1 and 3.7 MeV that do not seem to have transfers with $L > 0$ but are still difficult to assign surely as $L = 0$, since their shape, though forward peaking, is not typical. From the 2^+ states known up to about 2.4 MeV only the one at 2137 keV [10] was not populated in our reaction (almost unobservable). On the other hand, in a representation of the number of 2^+ states versus the excitation energy, the data start deviating from an exponential curve around 3.3 MeV. An exponential behavior is expected on the basis of simple formulas of the level densities, such as the constant temperature model, which are known to describe very well the data at low excitation energies [32,33]. Therefore, it is likely that above approximately 3.3 MeV we have missed some very weakly excited 2^+ states (see also the discussion below). With these observations, one may conclude that, for the 0^+ and 2^+ states, the (p, t) reaction study performed with high sensitivity and energy resolution may be considered a tool with a rather valuable contribution to the general quest of performing complete spectroscopy up to a medium density of states. Thus, the present data are interesting for a detailed testing of structure models.

C. Spectroscopic information

As outlined above, the experimental angular distributions were compared with DWBA calculations that assumed the same simple form factor for all states, corresponding to the two neutrons in the $2f_{7/2}$ orbital. This ensures a roughly correct treatment of both the kinematic (Q value) and configuration dependence effects, especially if the main neutron orbitals

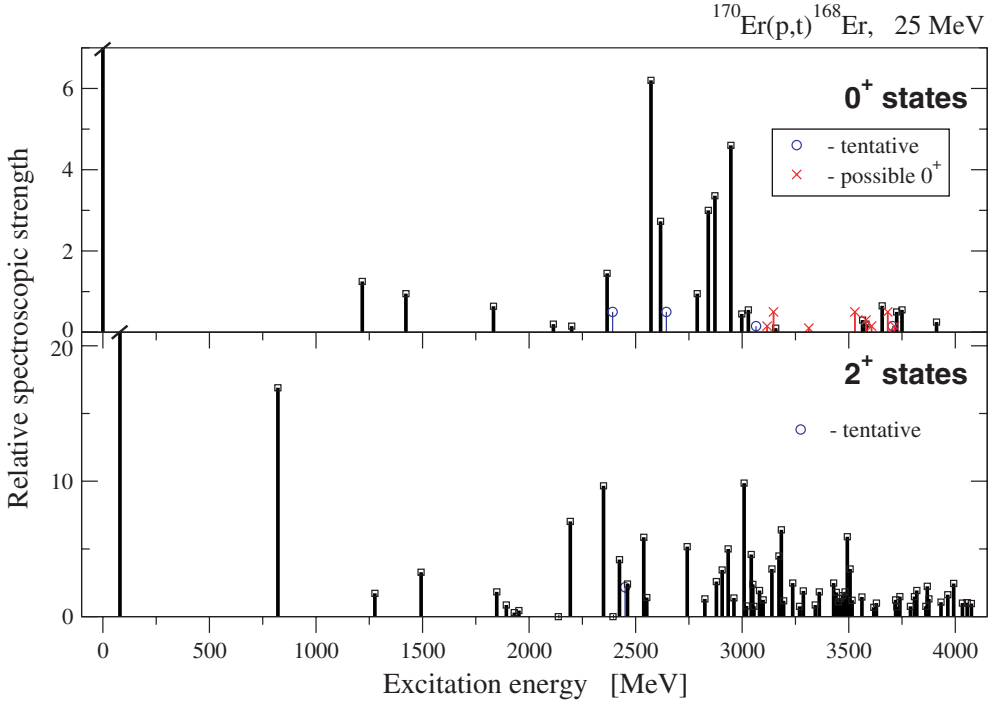

FIG. 6. (Color online) Relative (p, t) reaction transfer strengths (corresponding to a $f^2_{7/2}$ DWBA form factor; see discussion in the text) to 0^+ and 2^+ states in the ^{168}Er nucleus. The values for the 0^+ ground state and the 2^+_1 state at 79.8 keV, respectively, were normalized to 100 (Tables I and II).

involved in the transfer are, as expected, $2f_{7/2}$, $2f_{5/2}$, and $3p_{3/2}$ (see Fig. 2). The normalization of these calculated angular distributions to the experimental ones provides some relative (p, t) reaction transfer strength values. Naming these values "spectroscopic factors" is rather improper, but we may use these quantities just to have a rough image of how the (p, t) reaction strength is distributed over the experimental states. With this warning about the meaning of the experimental values that we extract from our data, we show in Fig. 6 the energy distribution of these quantities. The distribution of the 0^+ strength is rather different from that observed in ^{158}Gd [2] and other nuclei between ^{150}Sm and ^{180}Os [8]. There is no strongly excited 0^+ state at lower energies, and the integrated strength of the excited 0^+ states amounts to roughly 20% of the ground state strength. The 2^+_2 state at 821 keV is strongly populated. For both 0^+ and 2^+ states we observe some relatively larger strength with fragments distributed around 2.75 MeV excitation energy.

III. COMPARISON WITH MODEL CALCULATIONS

A. Quasiparticle-phonon model calculations

In the QPM model [23], microscopic phonons are generated in the random-phase approximation (RPA). Then, a Hamiltonian composed of a sum of separable two-body potentials with different multipolarities is diagonalized in a basis of multiphonon states. In the multiphonon basis, both collective and noncollective RPA phonons are included, and thus the model offers the possibility to determine the nature of the nuclear states. In QPM, one adopts a Hamiltonian composed of a deformed axially symmetric Woods-Saxon potential plus a two-body interaction of general separable form, acting

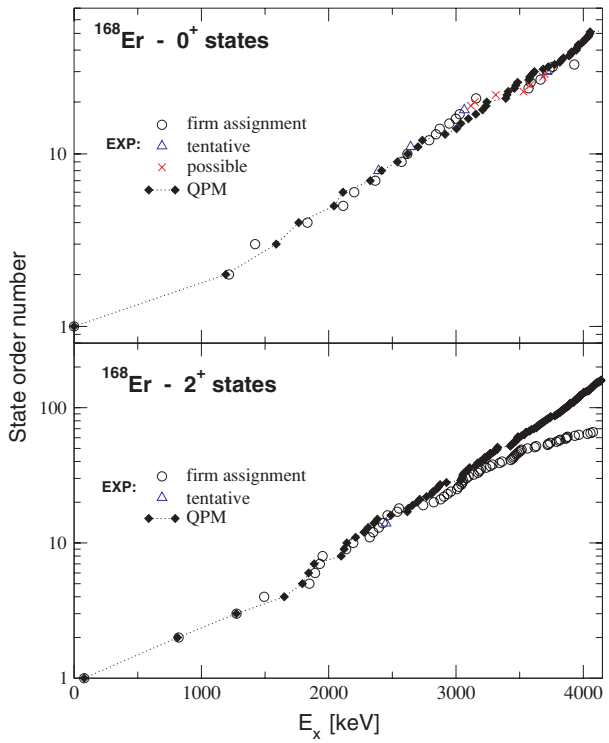

FIG. 7. (Color online) Comparison of experimental and calculated (QPM) 0^+ and 2^+ levels in ^{168}Er (note the logarithmic y-axis scale).

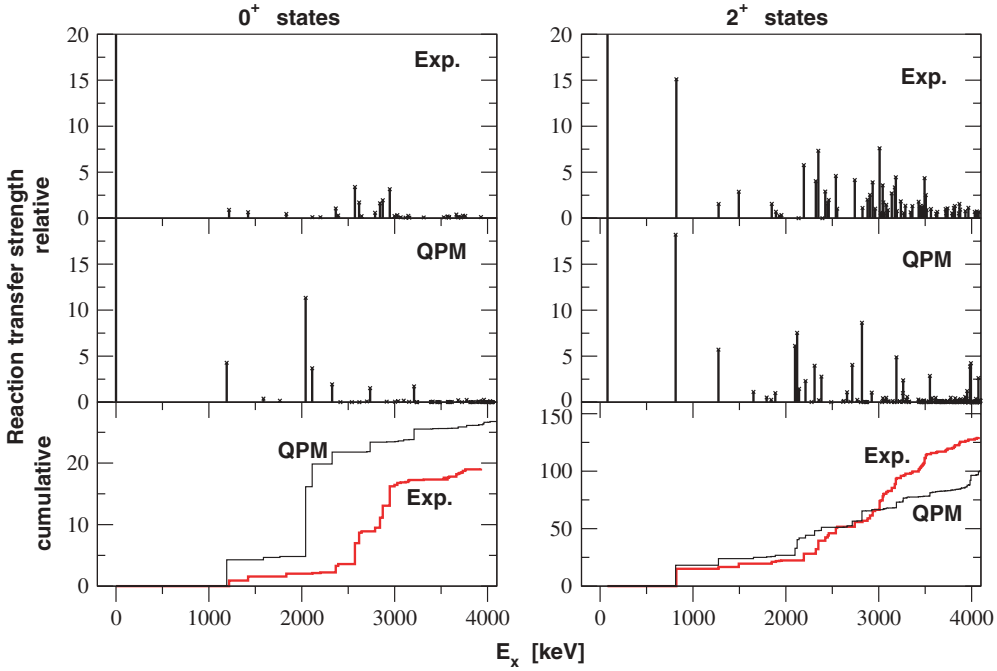

FIG. 8. (Color online) Comparison of experimental and calculated (QPM) 0^+ and 2^+ relative level reaction strengths for the (p, t) transfer. The values for the $0^+_{\text{g.s.}}$ and 2^+_1 states are normalized to 100.

in both particle-particle and particle-hole channels. The particle-particle interaction consists of a monopole plus a sum of λ multipole proton-proton and neutron-neutron pairing potentials. The particle-hole interaction is composed of a sum of proton-proton, neutron-neutron, and proton-neutron separable potentials of different multipolarity λ, including, among others, quadrupole-quadrupole and octupole-octupole pieces.

Following the QPM prescriptions [23], we express the above Hamiltonian in terms of the quasiparticle random-phase approximation (QRPA) phonon operators

$$Q^\dagger_{i\nu} = \frac{1}{2}\sum_{q_1 q_2}\left(\psi^{i\nu}_{q_1 q_2}\alpha^\dagger_{q_1}\alpha^\dagger_{\bar{q}_2} - \phi^{i\nu}_{q_1 q_2}\alpha_{\bar{q}_2}\alpha_{q_1}\right), \tag{1}$$

where the quasiparticle creation (annihilation) operators $\alpha^\dagger_q$ (α_q) are obtained from the corresponding particle operators $a^\dagger_q$ (a_q) through a Bogoliubov transformation.

The resulting Hamiltonian is then diagonalized in a space spanned by one- and two-phonon states, so that the QPM eigenstates as a result have the structure

$$\Psi_{nK} = \sum_i C^{(n)}_i Q^\dagger_{i\lambda K} \mid 0\rangle + \sum_{\nu_1\nu_2} C^{(n)}_{\nu_1\nu_2}\left[Q^\dagger_{\nu_1}\otimes Q^\dagger_{\nu_2}\right]_K \mid 0\rangle, \tag{2}$$

where $\lambda = 2$, $K = 0, 1, 2$, and ν_i labels the phonon quantum numbers. Each of these states represents the intrinsic component of the total wave function

$$\Psi^I_{nMK} = \sqrt{\frac{(1+\delta_{K0})(2I+1)}{16\pi^2}} \times \left[D^I_{MK}\Psi_{nK} + (-)^{I+K}D^I_{M-K}\Psi_{n\bar{K}}\right], \tag{3}$$

where D^I_{MK} is the Wigner matrix. The observed levels with angular momentum I are described by the $I = K$ bandhead states of positive parity with projection K onto the symmetry axis.

We use these wave functions to compute the (p, t) transfer normalized spectroscopic factors

$$\mathcal{S}_n(p,t) = \left[\frac{\Gamma_n(p,t)}{\Gamma_0(p,t)}\right]^2, \tag{4}$$

where, following Ref. [34], the amplitudes are given by

$$\Gamma_n(p,t) = \left\langle \Psi^I_{nMK}, N-2\right| \sum_{q_1 q_2} r^I Y_{IK} a_{q_1} a_{q_2} \left|\Psi_0, N\right\rangle. \tag{5}$$

The amplitude $\Gamma_0(p, t)$ refers to the transition to the I member of the ground state rotational band. More details of the calculations are given in Ref. [9].

The QPM yields more 0^+ and 2^+ excited states than the ones observed experimentally. The 0^+ and 2^+ states generated up to 4 MeV are 44 and 125, respectively, considerably more than the observed 25 (or 32, eventually, if we count also the possible 0^+ states shown in Fig. 4) and 66 corresponding experimental levels (Fig. 7). The excess states, however, lie above 3 MeV and carry too little strength to be detected experimentally. Figure 8 presents a comparison of the theoretical spectroscopic factors with the experimental reaction strengths. As was discussed above, the later quantities are only very crude approximations for the spectroscopic factors, so that this comparison should be taken only very qualitatively. As shown in Fig. 8, the calculation reproduces fairly well the magnitude and distribution of the two-nucleon transfer strength for both 0^+ and 2^+ states. As was remarked in Ref. [9], for the 0^+

TABLE III. Phonon structure of selected 2^+ QPM states. C_i^2 is the weight of the one-phonon ($[\lambda\mu]_i$) or the two-phonon ($[(\lambda\mu)_i(\lambda\mu)_j]_{2^+}$ components, denoted $[v_i]$. $S(p,t)$ is the (p,t) transfer spectroscopic factor normalized to the 2_1^+ state.

n	E_x	$S(p,t)$	$[v_i]$	$C_i^2(\%)$	n	E_x	$S(p,t)$	$[v_i]$	$C_i^2(\%)$
		$K=0$					$K=2$		
1	1.274	0.0571	$[20]_1$	55	1	0.813	0.182	$[22]_1$	94
			$[20]_2$	20	2	1.793	0.0051	$[22]_2$	86
			$[(22)_1(22)_1)]$	10	3	1.886	0.0099	$[22]_2$	8
2	1.651	0.0112	$[20]_1$	28				$[22]_5$	44
			$[20]_2$	63				$[(20)_1(22)_1)]$	19
3	1.842	0.0026	$[20]_3$	88				$[(22)_1(44)_1)]$	7
4	2.121	0.0753	$[20]_4$	73	4	2.098	0.0612	$[22]_3$	90
5	2.212	0.023	$[20]_4$	12	5	2.309	0.0397	$[22]_4$	83
			$[20]_5$	80	6	2.715	0.0405	$[22]_6$	70
6	2.383	0.0278	$[20]_4$	9				$[(20)_2(22)_1)]$	7
			$[20]_5$	7	7	2.768	0.0025	$[22]_5$	10
			$[20]_6$	48				$[22]_7$	49
			$[(22)_1(22)_1)]$	15				$[(32)_1(54)_1)]$	20
10	2.819	0.0863	$[20]_9$	86	8	2.924	0.0104	$[22]_8$	66
13	3.081	0.0049	$[20]_{12}$	7				$[(32)_1(54)_1)]$	11
			$[(31)_1(31)_1)]$	78	9	3.045	0.0043	$[22]_7$	14
		$K=1$						$[(20)_1(22)_1)]$	10
1	2.142	0.0145	$[21]_1$	82				$[(22)_1(44)_1)]$	13
			$[21]_3$	7				$[(32)_1(54)_1)]$	17
2	2.277	0.0002	$[21]_2$	93	10	3.054	0.0015	$[22]_8$	10
3	2.356	0.0022	$[21]_1$	12				$[(20)_1(22)_1)]$	10
			$[21]_3$	65				$[(22)_1(44)_1)]$	14
4	2.625	0.0013	$[21]_4$	81				$[(32)_1(54)_1)]$	33
5	2.659	0.0108	$[21]_3$	7	11	3.107	0.0002	$[(31)_1(33)_1)]$	81
			$[21]_5$	72	13	3.190	0.0488	$[22]_{11}$	29
								$[(20)_4(22)_1)]$	35

states the QPM reproduces rather correctly the total spectroscopic strength, although there are discrepancies concerning the strength of the strongest excited state and the centroid of the strength distribution (the predicted centroid is about 0.8 MeV lower in energy than observed). The truncation to no more than two phonon basis states may alter the predicted distribution and centroid, although it should not affect the integrated strength. For the 2^+ states, the distribution of the strength is rather well predicted up to about 3.0 MeV excitation. Above 3 MeV the calculation appears to start underestimating the collected strength, although the number of calculated states is much higher than that of the experimentally observed states. Again, inclusion of higher phonon states could shift some strength into this region via mixing.

It is of interest to examine the structure of the more strongly populated states. For the 0^+ states this has been done in detail in Ref. [9]; the main conclusion was that the 0^+ states in ^{168}Er below 3 MeV are mostly one-phonon states, sometimes fragmented, while above 3 MeV the weight of two-phonon components increases; all these states lack quadrupole collectivity. For the 2^+ states, we show some examples of phonon structures in Table III. One can see that these are dominantly fragmented one-phonon states with two-phonon admixtures. The one-phonon component is in general a linear combination of a dominant RPA component plus few other RPA configurations. The dominant RPA components are linear combinations of several two-quasineutron and (or) two-quasiproton states (Table IV). The structure of the predicted (p,t) spectra is the result of the phonon fragmetation on one hand, and, on the other hand, of the level of coherence of the two-quasiparticle amplitudes in each dominant RPA phonon.

B. Projected shell model calculations

A second theoretical calculation is performed with the projected shell model (PSM) [24], which is a truncated shell model based on deformed bases. The PSM calculation begins with a set of deformed Nilsson single-particle states [35] with a quadrupole deformation ε_2. Pairing correlations are incorporated into the Nilsson states by the BCS calculation. The Nilsson-BCS calculations define a set of quasiparticle (qp) states corresponding to the qp vacuum $|0\rangle$. One then constructs the shell model bases by building multi-qp states from those Nilsson orbitals that lie close to the Fermi levels. The broken rotational symmetry in the multi-qp states is recovered by exact angular momentum projection [24] to form a shell model basis in the laboratory frame. Finally a two-body shell model Hamiltonian is diagonalized in the projected space.

TABLE IV. Quasiparticle structure of the low-lying RPA quadrupole phonons.

n	E	$S(p,t)$	Structure	%	n	E	$S(p,t)$	Structure	%
		$K=0$					$K=1$		
1	1.647	0.0703	$\frac{5}{2}512\nu$, $\frac{5}{2}512\nu$	61	4	2.719	7.10^{-5}	$\frac{3}{2}521\nu$, $\frac{1}{2}521\nu$	91
			$\frac{7}{2}633\nu$, $\frac{7}{2}633\nu$	22				$\frac{5}{2}512\nu$, $\frac{3}{2}521\nu$	6
2	1.695	0.0003	$\frac{1}{2}521\nu$, $\frac{1}{2}521\nu$	61	5	2.753	0.011	$\frac{5}{2}512\nu$, $\frac{3}{2}521\nu$	39
			$\frac{7}{2}633\nu$, $\frac{7}{2}633\nu$	25				$\frac{3}{2}521\nu$, $\frac{1}{2}521\nu$	6
			$\frac{5}{2}512\nu$, $\frac{5}{2}512\nu$	13			$K=2$		
3	1.901	0.0003	$\frac{1}{2}411\pi$, $\frac{1}{2}411\pi$	45	1	0.945	0.1822	$\frac{5}{2}523\nu$, $\frac{1}{2}521\nu$	23
			$\frac{7}{2}523\pi$, $\frac{7}{2}523\pi$	27				$\frac{3}{2}521\nu$, $\frac{1}{2}521\nu$	14
			$\frac{3}{2}411\pi$, $\frac{3}{2}411\pi$	11				$\frac{5}{2}512\nu$, $\frac{1}{2}510\nu$	7
4	2.130	0.1502	$\frac{5}{2}523\nu$, $\frac{5}{2}523\nu$	33				$\frac{3}{2}411\pi$, $\frac{1}{2}411\pi$	17
			$\frac{7}{2}633\nu$, $\frac{7}{2}633\nu$	22				$\frac{5}{2}413\pi$, $\frac{1}{2}411\pi$	5
			$\frac{5}{2}642\nu$, $\frac{5}{2}642\nu$	18	2	1.952	0.0009	$\frac{5}{2}512\nu$, $\frac{1}{2}521\nu$	98
			$\frac{1}{2}521\nu$, $\frac{1}{2}521\nu$	9	3	2.198	0.0649	$\frac{5}{2}523\nu$, $\frac{1}{2}521\nu$	60
			$\frac{3}{2}521\nu$, $\frac{3}{2}521\nu$	6				$\frac{3}{2}411\pi$, $\frac{1}{2}411\pi$	36
5	2.265	2.10^{-5}	$\frac{5}{2}512\nu$, $\frac{5}{2}523\nu$	98	4	2.438	0.0859	$\frac{3}{2}521\nu$, $\frac{1}{2}521\nu$	59
6	2.509	1.10^{-5}	$\frac{7}{2}404\pi$, $\frac{7}{2}404\pi$	32				$\frac{5}{2}523\nu$, $\frac{1}{2}521\nu$	11
			$\frac{9}{2}514\pi$, $\frac{9}{2}514\pi$	28				$\frac{3}{2}411\pi$, $\frac{1}{2}411\pi$	26
			$\frac{1}{2}411\pi$, $\frac{1}{2}411\pi$	17	5	2.743	0.0031	$\frac{5}{2}512\nu$, $\frac{1}{2}510\nu$	34
			$\frac{3}{2}411\pi$, $\frac{3}{2}411\pi$	11				$\frac{3}{2}521\nu$, $\frac{1}{2}521\nu$	21
7	2.571	8.10^{-6}	$\frac{3}{2}411\pi$, $\frac{3}{2}411\pi$	53				$\frac{7}{2}514\nu$, $\frac{3}{2}512\nu$	7
			$\frac{7}{2}523\pi$, $\frac{7}{2}523\pi$	34				$\frac{9}{2}624\nu$, $\frac{5}{2}642\nu$	6
8	2.753	0.0094	$\frac{9}{2}624\nu$, $\frac{9}{2}624\nu$	55				$\frac{3}{2}411\pi$, $\frac{1}{2}411\pi$	10
			$\frac{7}{2}514\nu$, $\frac{7}{2}514\nu$	27	6	2.942	0.0307	$\frac{7}{2}633\nu$, $\frac{3}{2}651\nu$	86
			$\frac{5}{2}512\nu$, $\frac{5}{2}512\nu$	8				$\frac{5}{2}512\nu$, $\frac{1}{2}510\nu$	6
9	2.812	0.0807	$\frac{5}{2}523\nu$, $\frac{5}{2}523\nu$	48	7	3.063	0.0033	$\frac{9}{2}624\nu$, $\frac{5}{2}642\nu$	33
			$\frac{5}{2}642\nu$, $\frac{5}{2}642\nu$	43				$\frac{5}{2}512\nu$, $\frac{1}{2}510\nu$	11
		$K=1$						$\frac{5}{2}413\pi$, $\frac{1}{2}411\pi$	43
1	2.199	0.0184	$\frac{7}{2}633\nu$, $\frac{5}{2}642\nu$	80	8	3.111	0.0101	$\frac{9}{2}624\nu$, $\frac{5}{2}642\nu$	58
			$\frac{9}{2}624\nu$, $\frac{7}{2}633\nu$	13				$\frac{5}{2}413\pi$, $\frac{1}{2}411\pi$	39
2	2.338	2.10^{-9}	$\frac{3}{2}411\pi$, $\frac{1}{2}411\pi$	98	11	3.759	0.1432	$\frac{5}{2}642\nu$, $\frac{1}{2}660\nu$	76
3	2.539	0.0011	$\frac{9}{2}624\nu$, $\frac{7}{2}633\nu$	62				$\frac{3}{2}532\nu$, $\frac{1}{2}521\nu$	5
			$\frac{5}{2}512\nu$, $\frac{3}{2}521\nu$	7					
			$\frac{9}{2}514\pi$, $\frac{7}{2}523\pi$	24					

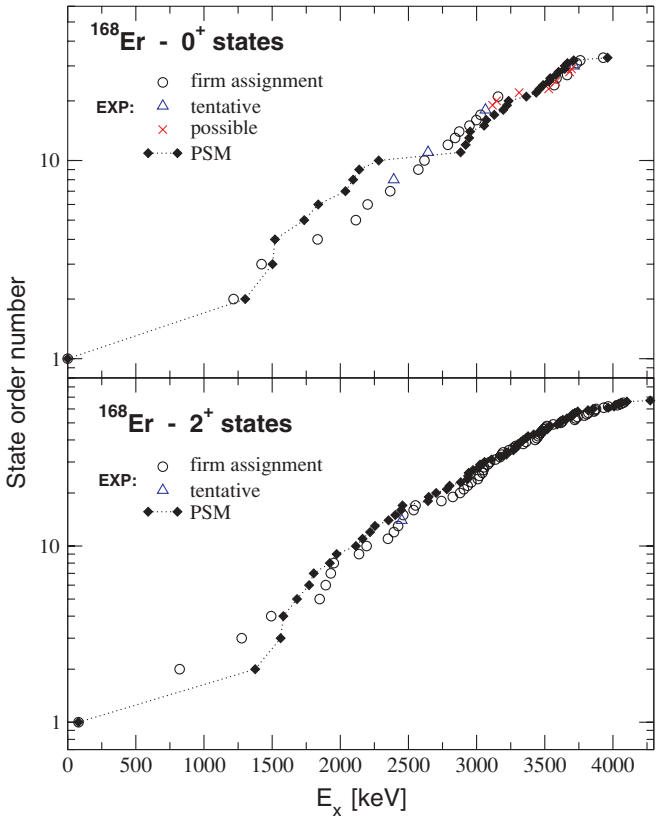

FIG. 9. (Color online) Comparison of experimental and calculated (PSM) 0^+ and 2^+ levels.

The PSM wave function is a superposition of projected multi-qp states that form the shell model basis

$$\left|\psi_M^I\right\rangle = \sum_\kappa f_\kappa^I \hat{P}_{MK_\kappa}^I \left|\phi_\kappa\right\rangle . \tag{6}$$

Here, κ labels the basis states and f_κ^I are determined by the configuration mixing implemented by diagonalization. $\hat{P}_{MK_\kappa}^I$ is the angular-momentum projection operator [36], which projects an intrinsic configuration $|\phi_\kappa\rangle$ onto states with good angular momentum. As in many previous PSM calculations for the rare-earth nuclei, particles in three major shells ($N = 4, 5, 6$ for neutrons and $N = 3, 4, 5$ for protons) are included in the present calculation. The construction of $|\phi_\kappa\rangle$ follows the spirit of the Tamm-Dancoff approximation [36], in which one builds the model space by including 0-, 2- and 4-qp states:

$$|\Phi_\kappa\rangle = \left\{ |0\rangle , \alpha_{n_i}^\dagger \alpha_{n_j}^\dagger |0\rangle , \alpha_{p_k}^\dagger \alpha_{p_l}^\dagger |0\rangle , \alpha_{n_i}^\dagger \alpha_{n_j}^\dagger \alpha_{p_k}^\dagger \alpha_{p_l}^\dagger |0\rangle \right\} , \tag{7}$$

where $\alpha^\dagger$ is the creation operator for a qp and the index n (p) denotes neutron (proton) Nilsson quantum numbers, which run over the low-lying orbitals. The model space is truncated by excluding those multi-qp states having energies higher than 4.4 MeV.

One then diagonalizes the Hamiltonian in the projected multi-qp states given in Eq. (6). In the calculation, we employ a quadrupole-plus-pairing Hamiltonian, with inclusion of the

TABLE V. Main components in the 0^+ states (below 4 MeV) in ^{168}Er as calculated by the projected shell model.

Order number	E (MeV)	qp states	Configurations
1	1.302	2-qp	$-\frac{1}{2}[521]\nu$, $\frac{1}{2}[521]\nu$
2	1.503	2-qp	$-\frac{7}{2}[523]\pi$, $\frac{7}{2}[523]\pi$
3	1.521	2-qp	$-\frac{7}{2}[633]\nu$, $\frac{7}{2}[633]\nu$
4	1.735	2-qp	$-\frac{1}{2}[411]\pi$, $\frac{1}{2}[411]\pi$
5	1.838	2-qp	$-\frac{5}{2}[512]\nu$, $\frac{5}{2}[512]\nu$
6	2.038	2-qp	$-\frac{5}{2}[523]\nu$, $\frac{5}{2}[523]\nu$
7	2.094	2-qp	$-\frac{5}{2}[512]\nu$, $\frac{5}{2}[523]\nu$
8	2.139	2-qp	$-\frac{7}{2}[404]\pi$, $\frac{7}{2}[404]\pi$
9	2.281	2-qp	$-\frac{3}{2}[411]\pi$, $\frac{3}{2}[411]\pi$
10	2.822	4-qp	$-\frac{1}{2}[521]\nu$, $\frac{1}{2}[521]\nu$, $-\frac{7}{2}[523]\pi$, $\frac{7}{2}[523]\pi$
11	2.920	2-qp	$-\frac{5}{2}[402]\pi$, $\frac{5}{2}[402]\pi$
12	2.946	4-qp	$-\frac{1}{2}[521]\nu$, $\frac{1}{2}[521]\nu$, $-\frac{1}{2}[411]\pi$, $\frac{1}{2}[411]\pi$
13	2.953	4-qp	$-\frac{7}{2}[633]\nu$, $\frac{7}{2}[633]\nu$, $-\frac{7}{2}[523]\pi$, $\frac{7}{2}[523]\pi$
14	3.005	4-qp	$-\frac{7}{2}[633]\nu$, $\frac{7}{2}[633]\nu$, $-\frac{1}{2}[411]\pi$, $\frac{1}{2}[411]\pi$
15	3.071	2-qp	$-\frac{11}{2}[505]\nu$, $\frac{11}{2}[505]\nu$
16	3.130	2-qp	$-\frac{5}{2}[413]\pi$, $\frac{5}{2}[413]\pi$
17	3.196	2-qp	$-\frac{5}{2}[642]\nu$, $\frac{5}{2}[642]\nu$
18	3.223	2-qp	$-\frac{7}{2}[514]\nu$, $\frac{7}{2}[514]\nu$
19	3.235	2-qp	$-\frac{5}{2}[402]\pi$, $\frac{5}{2}[413]\pi$
20	3.365	4-qp	$-\frac{5}{2}[512]\nu$, $\frac{5}{2}[512]\nu$, $-\frac{7}{2}[523]\pi$, $\frac{7}{2}[523]\pi$
21	3.437	4-qp	$-\frac{5}{2}[512]\nu$, $-\frac{5}{2}[512]\nu$, $\frac{1}{2}[411]\pi$, $\frac{1}{2}[411]\pi$
22	3.462	4-qp	$-\frac{1}{2}[521]\nu$, $\frac{1}{2}[521]\nu$, $-\frac{7}{2}[404]\pi$, $\frac{7}{2}[404]\pi$
23	3.488	2-qp	$-\frac{9}{2}[514]\pi$, $\frac{9}{2}[514]\pi$
24	3.530	4-qp	$-\frac{1}{2}[521]\nu$, $\frac{1}{2}[521]\nu$, $-\frac{3}{2}[411]\pi$, $\frac{3}{2}[411]\pi$
25	3.540	4-qp	$-\frac{5}{2}[512]\nu$, $\frac{5}{2}[523]\nu$, $-\frac{7}{2}[523]\pi$, $\frac{7}{2}[523]\pi$
26	3.582	4-qp	$-\frac{5}{2}[523]\nu$, $\frac{5}{2}[523]\nu$, $-\frac{7}{2}[523]\pi$, $\frac{7}{2}[523]\pi$
27	3.601	4-qp	$-\frac{7}{2}[633]\nu$, $\frac{7}{2}[633]\nu$, $-\frac{7}{2}[404]\pi$, $\frac{7}{2}[404]\pi$
28	3.647	4-qp	$-\frac{7}{2}[633]\nu$, $\frac{7}{2}[633]\nu$, $-\frac{3}{2}[411]\pi$, $\frac{3}{2}[411]\pi$
29	3.647	4-qp	$-\frac{5}{2}[512]\nu$, $\frac{5}{2}[523]\nu$, $-\frac{1}{2}[411]\pi$, $\frac{1}{2}[411]\pi$
30	3.667	2-qp	$-\frac{5}{2}[532]\pi$, $\frac{5}{2}[532]\pi$
31	3.712	4-qp	$-\frac{1}{2}[521]\nu$, $-\frac{5}{2}[512]\nu$, $-\frac{1}{2}[411]\pi$, $\frac{7}{2}[404]\pi$
32	3.961	2-qp	$-\frac{1}{2}[521]\nu$, $\frac{1}{2}[510]\nu$

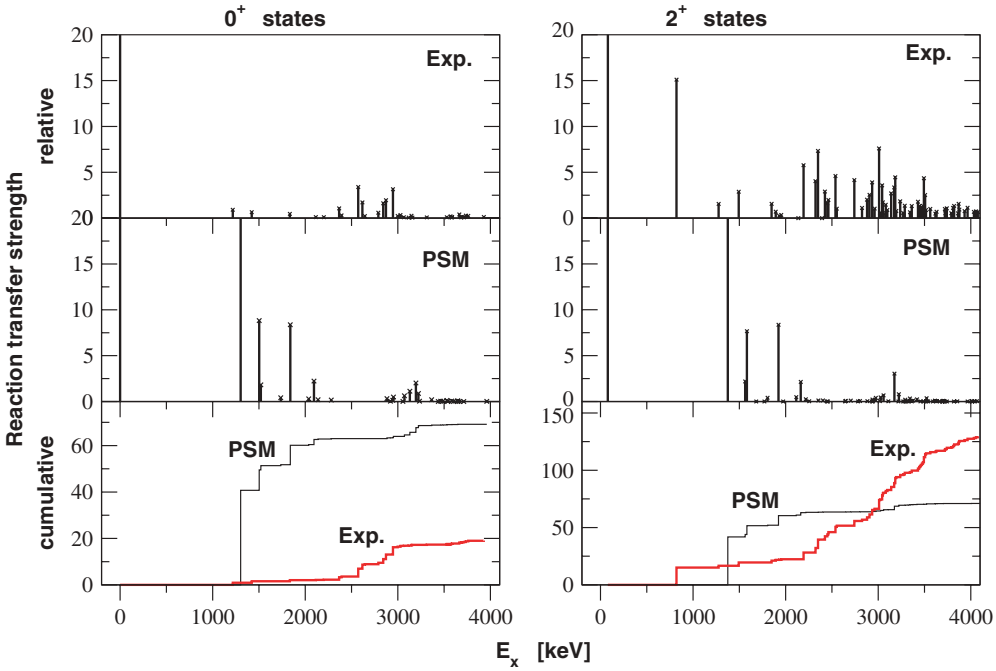

FIG. 10. (Color online) Comparison of experimental and calculated (PSM) 0^+ and 2^+ relative level reaction strengths for the (p, t) transfer. The values for the $0^+_{\text{g.s.}}$ and 2^+_1 states are normalized to 100.

quadrupole-pairing term

$$\hat{H} = \hat{H}_0 - \frac{1}{2}\chi \sum_{\mu} \hat{Q}^\dagger_\mu \hat{Q}_\mu - G_M \hat{P}^\dagger \hat{P} - G_Q \sum_{\mu} \hat{P}^\dagger_\mu \hat{P}_\mu. \quad (8)$$

In Eq. (8), $\hat{H}_0$ is the spherical single-particle Hamiltonian, which contains a proper spin-orbit force. The quadrupole-quadrupole interaction strength χ is determined by the self-consistent relation with deformation ε_2, and $\varepsilon_2 = 0.273$ in the present calculation for ^{168}Er. The monopole pairing strength G_M is taken to be $G_M = [21.24 - 13.13(N \mp Z)/A]/A$ with a $-$ sign for neutrons and $+$ sign for protons. Finally, the quadrupole pairing strength G_Q is assumed to be proportional to G_M, the proportionality constant being fixed to 0.16 in the present work. These interaction strengths are the same as the values used in the previous PSM calculations for many rare-earth nuclei [4] and, in particular, are the same as the early theoretical work on ^{168}Er [37], although the physical phenomenon (multiphonon γ vibrational states) discussed there is quite different.

The PSM calculations are compared with data in Fig. 9 in a plot of the number of states versus excitation energy. Good agreement seems to be obtained. In particular, there is a remarkable similarity between the theoretical results and experimental data for the 2^+ states. (The calculation does not show the first excited 2^+ state, which is the γ-vibrational band-head, because the vibrational degree of freedom is not included in the present PSM model space). This similarity tends to suggest that the number of observed states in the present (p, t) experiment is very close to the number of possible multi-qp states that can be constructed in the PSM model space. In Table V we list the configurations for the theoretical 2- and 4-qp states from the 0^+ calculations. Two remarks are in order. First, these multi-qp states are built on top of the qp vacuum plus angular momentum projection that effectively accounts for the couplings between the rotating body and the quasiparticles in a quantum-mechanical way. Second, the projected multi-qp states are mixed in the subsequent procedure of solving the eigenvalue equation. Therefore the configurations listed in Table V mean solely the main component in each state. The states finally obtained in the PSM calculations thus should not be regarded as single-particle states in the mean-field sense.

We comment on the total number of the states below 4 MeV. Of course, one can speculate that there may be states that are insensitive to the (p, t) excitation and that therefore are not seen in the present experiment. In fact, as shown above, the QPM predicts more states in the higher excitation region than the data show (and more than the PSM prediction). In this regard, it should be mentioned that in the current PSM model space in Eq. (7), we do not consider the 4-qp states with four like particles. This is, the configurations $\{\alpha^\dagger_{n_i}\alpha^\dagger_{n_j}\alpha^\dagger_{n_k}\alpha^\dagger_{n_l}|0\rangle\}$ and $\{\alpha^\dagger_{p_i}\alpha^\dagger_{p_j}\alpha^\dagger_{p_k}\alpha^\dagger_{p_l}|0\rangle\}$ are not included. These configurations lie generally higher, but for an excitation close to 4 MeV, some of the missing states may fall into that energy range. If these states were taken into account, the total number of states would increase.

We use the obtained wave functions to calculate the normalized spectroscopic factors of Eq. (4), and the results are compared with the data in Fig. 10. We recall again that because of the way we extract the experimental reaction strengths, this comparison must be considered only at a very qualitative level. With the present model space it is difficult to describe

the observations. The main discrepancy is that the theoretical strengths concentrate incorrectly in a few low-lying states. This suggests that, although the PSM energy levels match the data reasonably well, the content of the wave functions is incorrect. The space truncation that allows multi-qp states below 4.4 MeV in the configuration mixing excludes the possibility of any influence from the large body of the higher-lying states, resulting in an insufficient coherence in the low-lying states. On the other hand, as seen in the discussion of the previous section, the QPM, whose states are highly coherent by construction, can describe the experimental spectroscopic factors much better. Comparing the results of QPM and PSM, one may conclude that many low-lying 0^+ and 2^+ states in ^{168}Er are coherent in nature. This property is missing in the present PSM calculation that uses only a small set of quasiparticle states in its model space.

IV. CONCLUSIONS

We have presented a detailed investigation of excited states of the deformed nucleus ^{168}Er with a high-resolution (p, t) transfer reaction experiment. Clear assignments of a large number of 0^+ and 2^+ states have been made up to 4.1 MeV excitation. It is argued that up to about 3.3 MeV excitation a practically complete determination of the 0^+ and 2^+ excitations was achieved. This shows that such a high-resolution, background-free experiment, although performed with a reaction that has a certain selectivity in the structure of the populated final states, is able to provide a quasi-complete determination of such low-spin levels up to excitation energies with a moderate to high level density.

The large number of observed 0^+ and 2^+ levels allows a detailed comparison with predictions of microscopic structure models. Two such approaches are discussed and compared with the data: the quasiparticle-phonon model (QPM), and the projected shell model (PSM). The QPM predicts well the number and distribution in energy of both the 0^+ and 2^+ states. In the case of the 2^+ states, the number of states predicted above 3.2 MeV is larger than observed, many of these states being predicted with rather small (p, t) spectroscopic strengths. The reaction strengths for the 0^+ states are qualitatively reproduced: the main discrepancy is a shift, of about 0.7 MeV toward lower energies, of a group of stronger populated levels that are experimentally observed around 2.7 MeV. The distribution of the 2^+ strengths is well reproduced up to about 3 MeV, after which they may be underestimated by the calculations. Thus, in the present QPM calculations there are still missing configurations that are important up to 4 MeV excitation. The PSM calculations, which do not explicitly include vibrational degrees of freedom in the present approach, also describe reasonably well the number and energy distribution of the 0^+ and 2^+ levels. However, the predicted distribution of the reaction strength is concentrated mostly in several low-lying (up to about 2 MeV) excited states, which does not fit the experimental observations, where it is fragmented over a larger number of states. This indicates that the PSM states, which have correctly reproduced the energy levels, lack the higher coherence required by the data.

Because of the fragmentation in the phonon and quasiparticle structure of the QPM states, it is very difficult to state a relation between QPM and PSM. We can only say that the QPM states are highly correlated, though not necessarily collective, linear combinations of two- and four-quasiparticle states. The PSM states, unlike the QPM ones, do not contain such correlations before configuration mixing, and any of such correlations can only be brought in by diagonalization. Thus the present work has revealed the interesting fact that in order to describe the coherence discussed in this paper the PSM should consider the contribution from many more qp states than it is usually taken.

In conclusion, the detailed experimental knowledge of the 0^+ and 2^+ excitations in a deformed nucleus, ^{168}Er, has been enormously extended by the present measurements. The data extend up to a rather high excitation energy. Comparison with microscopic models clearly indicates some of their limitations. These data therefore constitute a valuable checkpoint for future calculations.

ACKNOWLEDGMENTS

We thank F. Iachello and T. von Egidy for useful discussions. D. Bucurescu acknowledges support within the Deutsche Forschungsgemeinschaft (DFG) grant II C4-GR894/1-3. This work was partly supported by the Romanian Ministry for Education and Research under contract CEX-05-D11-30, by the DFG grant 391/JO/2-3, by the National Science Foundation under contract PHY-0140324, and by the U.S. Department of Energy under grant DE-FG02-91ER-40609.

[1] P. E. Garrett, J. Phys. G: Nucl. Part. Phys. **27**, R1 (2001).
[2] S. R. Lesher, A. Aprahamian, L. Trache, A. Oros-Peusquens, S. Deyliz, A. Gollwitzer, R. Hertenberger, B. D. Valnion, and G. Graw, Phys. Rev. C **66**, 051305(R) (2002).
[3] N. V. Zamfir, J.-y. Zhang, and R. F. Casten, Phys. Rev. C **66**, 057303 (2002).
[4] Y. Sun, A. Aprahamian, J.-y. Zhang, and C.-T. Lee, Phys. Rev. C **68**, 061301(R) (2003).
[5] N. Lo Iudice, A. V. Sushkov, and N. Y. Shirikova, Phys. Rev. C **70**, 064316 (2004).
[6] M. Gerçeklioglu, Eur. Phys. J. A **25**, 185 (2005).
[7] H.-F. Wirth, G. Graw, S. Christen, D. Cutoiu, Y. Eisermann, C. Günther, R. Hertenberger, J. Jolie, A. I. Levon, O. Möller, G. Thiamova, P. Thirolf, D. Tonev, and N. V. Zamfir, Phys. Rev. C **69**, 044310 (2004).
[8] D. A. Meyer, G. Graw, R. Hertenberger, H.-F. Wirth, R. F. Casten, P. von Brentano, D. Bucurescu, S. Heinze, J. L. Jerke, J. Jolie, R. Krücken, M. Mahgoub, P. Pejovic, O. Möller, D. Mücher, and C. Scholl, J. Phys. G: Nucl. Part. Phys. **31**, S1399 (2005); D. A. Meyer *et al.* (to be published).

[9] N. Lo Iudice, A. V. Sushkov, and N. Y. Shirikova, Phys. Rev. C **72**, 034303 (2005).
[10] V. S. Shirley, Nucl. Data Sheets **71**, 261 (1994); ENSDF data base at http://www.nndc.bnl.gov.
[11] D. G. Burke, W. F. Davidson, J. A. Cizewski, R. E. Brown, E. R. Flynn, and J. W. Sunier, Can. J. Phys. **63**, 1309 (1985).
[12] W. F. Davidson *et al*., J. Phys. G **7**, 455 (1981); Addendum /Corrigendum *ibid*. **7**, 843 (1981).
[13] A. Jungclaus, R. F. Casten, R. L. Gill, and H. G. Börner, Phys. Rev. C **49**, 88 (1994).
[14] R. L. Gill, R. F. Casten, W. R. Phillips, B. J. Varley, C. J. Lister, J. L. Durell, J. A. Shannon, and D. D. Warner, Phys. Rev. C **54**, 2276 (1996).
[15] W. F. Davidson and W. R. Dixon, J. Phys. G: Nucl. Part. Phys. **17**, 1683 (1991).
[16] J. Rekstad, T. S. Tveter, and M. Guttormsen, Phys. Rev. Lett. **65**, 2122 (1990); J. Rekstad, T. S. Tveter, M. Guttormsen, and L. Bergholt, Phys. Rev. C **47**, 2621 (1993).
[17] B. R. Barrett, R. F. Casten, J. N. Ginocchio, T. Seligman, and H. A. Weidenmüller, Phys. Rev. C **45**, R1417 (1992).
[18] H. G. Börner, J. Jolie, S. J. Robinson, B. Krusche, R. Piepenbring, R. F. Casten, A. Aprahamian, and J. P. Draayer, Phys. Rev. Lett. **66**, 691 (1991).
[19] X. Wu, A. Aprahamian, S. M. Fischer, W. Reviol, G. Liu, and J. X. Saladin, Phys. Rev. C **49**, 1837 (1994).
[20] H. Lehmann, J. Jolie, F. Corminboeuf, H. G. Börner, C. Doll, M. Jentschel, R. F. Casten, and N. V. Zamfir, Phys. Rev. C **57**, 569 (1998).
[21] H. Maser, S. Lindenstruth, I. Bauske, O. Beck, P. von Brentano, T. Eckert, H. Friedrichs, R. D. Heil, R.-D. Herzberg, A. Jung, U. Kneissl, J. Margraf, N. Pietralla, H. H. Pitz, C. Wesselborg, and A. Zilges, Phys. Rev. C **53**, 2749 (1996).
[22] F. Iachello, Phys. Rev. Lett. **91**, 132502 (2003).
[23] V. G. Soloviev, *Theory of Atomic Nuclei: Quasiparticles and Phonons* (Institute of Physics, Bristol, 1992).
[24] K. Hara and Y. Sun, Int. J. Mod. Phys. E **4**, 637 (1997).
[25] M. Löffler, H. J. Scheerer, and H. Vonach, Nucl. Instrum. Methods **111**, 1 (1973).
[26] H.-F. Wirth, H. Angerer, T. von Egidy, Y. Eisermann, G. Graw, and R. Hertenberger, Beschleunigerlaboratorium München Annual Report, 2000, p. 71.
[27] H.-F. Wirth, Ph.D. thesis, Techn. Univ. München, 2001 (http://tumbl.biblio.tu-muenchen.de/publ/diss/ph/2001/wirth.html).
[28] C. M. Baglin, Nucl. Data Sheets **96**, 611 (2002); ENSDF data base at http://www.nndc.bnl.gov.
[29] E. Browne, Nucl. Data Sheets **88**, 29 (1999); ENSDF data base at http://www.nndc.bnl.gov.
[30] P. D. Kunz, Computer code CHUCK3, University of Colorado (unpublished).
[31] C. M. Perey and F. G. Perey, At. Data Nucl. Data Tables **17**, 1 (1976).
[32] T. von Egidy, A. N. Behkami, and H. H. Schmidt, Nucl. Phys. **A454**, 109 (1986); T. von Egidy, H. H. Schmidt, and A. N. Behkami, Nucl. Phys. **A481**, 189 (1988).
[33] T. von Egidy and D. Bucurescu, Phys. Rev. C **72**, 044311 (2005).
[34] R. A. Broglia, C. Riedel, and T. Udagawa, Nucl. Phys. **A135**, 561 (1969).
[35] C. G. Andersson, G. Hellström, G. Leander, I. Ragnarsson, S. Aberg, J. Krumlinde, S. G. Nilsson, and Z. Szymański, Nucl. Phys. **A309**, 141 (1978).
[36] P. Ring and P. Schuck, *The Nuclear Many Body Problem* (Springer-Verlag, New York, 1980).
[37] Y. Sun, K. Hara, J. A. Sheikh, J. G. Hirsch, V. Velázquez, and M. Guidry, Phys. Rev. C **61**, 064323 (2000).